SEISMIC DECONVOLUTION WITH SHEARLET SPARSITY CONSTRAINED INVERSION

CHENGMING LIU, DELI WANG, BIN HU and TONG WANG

College of Geo-Exploration Science and Technology, Jilin University, Changchun 130026, Jilin, P.R. China. liucm13@mails.jlu.edu.cn; wangdl@jlu.edu.cn

(Received September 6, 2015; revised version accepted June 28, 2016)

ABSTRACT

Liu, C., Wang, D., Hu, B. and Wang, T., 2016. Seismic deconvolution with shearlet sparsity constrained inversion. *Journal of Seismic Exploration*, 25: 433-445.

The application of conventional deconvolution methods must be under some assumptions, meanwhile the processing procedure is through single trace cycle, which may destroy the continuity of seismic events. Besides, these methods are serious interfered by noise. For these reasons, we proposed seismic deconvolution based on multiscale and multidirectional shearlet transform sparsity constrained inversion. Shearlet has the ability to represent multidimensional signals with optimal sparse representation. We expressed the reflected signals sparse characteristic by the sparse shearlet coefficients. Deconvolution based on multi-dimensional space transform maintains the continuity along reflectors theoretically compared to the traditional single channel method. We expressed the deconvolution problem as a l_1-norm optimization problem and combined with a fast iterative thresholding algorithm. Experiments on synthetic and field seismic data show our method could improve the resolution of seismic data effectively, attenuate random noise and make the events more smoothly.

KEY WORDS: shearlet transform, sparse deconvolution, l_1-norm minimum, resolution.

INTRODUCTION

Seismic deconvolution plays a vital role in improving vertical resolution of seismic data. The results of deconvolution directly affect the subsequent stack, migration and geological interpretation. Currently, the exploration areas are more focused on smaller and deeper buried reservoirs, while the conventional deconvolution methods cannot meet the requirements of high resolution.

0963-0651/16/$5.00

The application of conventional deconvolution methods such as least square deconvolution (Berkhout, 1977), spike deconvolution and prediction deconvolution are under some assumptions, such as minimum phase wavelet and Gaussian white reflectivity coefficients sequence. However, these conditions are often not satisfied in practice. Ulrych (1971) introduced an homomorphic system into deconvolution, which does not require the assumptions of minimum phase wavelet and Gaussian white reflectivity coefficients. Claerbout and Muir (1973) proposed to use the l_1-norm instead of least square to achieve more stable solutions. Gray (1979) put forward a variable norm deconvolution method, which estimates the reflectivity coefficients by minimum l_p-norm between the input and the desired output. Although the variable norm deconvolution has no special wavelet requirements, the sparse reflectivity coefficient is required, and it is severe interference by noise.

In order to reduce the noise influence on deconvolution, Oldenburg et al. (1981) proposed to use prior information or constraints to guarantee the accuracy of the result. Shlomo and Peter (1981) utilized the spectral information of seismic data to recover reflectivity using the l_1-norm, which gets quality of anti-noise. Kaaresen and Taxt (1998) described the deconvolution problem in a Bayesian framework. Canadas (2002) presented a scheme for blind deconvolution problems that the probability distribution of the reflectivity sequence was used as the penalty term. In this way both the wavelet and reflectivity sequence are simultaneously estimated. Nojadeh and Sacchi (2013) developed a Sparse Multichannel Blind Deconvolution method, which can tolerate moderate levels of noise and does not require a priori knowledge of the length of the wavelet.

Herrmann (2005) pointed out that it is too simple to represent seismic reflectivity coefficients as sparse spike in deconvolution. He proposed a redundant dictionary to describe the seismic reflectivity, which abandoned restrictions of the traditional assumptions. Hennenfent et al. (2005) proposed an iterative curvelet-regularized deconvolution algorithm that exploits continuity along reflectors in seismic images. Curvelet transform was introduced to represent non-spiky reflectivity by Meng and Wang (2013). Based on this method, we describe the deconvolution in the sparse transform domain and introduce shearlet transform into deconvolution. Shearlet is proved to have the optimal sparse representation of 2D data (Guo and Labate, 2007). In our method, the stratum reflective layers (faults or pinch-outs) could be seen as piecewise smooth curved reflective layer, whose reflectivity can be represented by the sparse Shearlet coefficients. We don't make the hypothesis of sparse reflectivity coefficients but use the sparse shearlet coefficients instead. Moreover, according to the distribution characteristics of the reflect signal and random noise in the shearlet domain, we apply a threshold algorithm to separate noise from the signal. In this way, we could improve resolution and suppress noise at the same time. Deconvolution based on multi-dimensional space

transform maintains the continuity along events in theoretically compared to the traditional single channel method, which combined the shearlet deconvolution problem with fast iterative thresholding algorithm (Beck and Teboulle, 2009). Numerical examples show that our method is robust and effective.

THEORY OF SHEARLET TRANSFORM

Shearlet transform is first introduced by Labate and Kutyniok (2005), which is obtained by applying the actions of dilation, shear transformation and translation to a fixed function, and exhibit the geometric and mathematical properties, e.g., directionality, elongated shapes, scales, oscillations, recently advocated by many authors for sparse image processing applications. Indeed, unlike wavelet generated by isotropic dilations, shearlets provide an optimal sparse representation of anisotropic and directional information at multiscales.

Shearlet systems are generated by a parabolic scaling, translation and shearing operators to change the orientation. A shearlet system is built from a generating function $\varphi(t)$ by orienting it using $\mathbf{S}_s$, scaling it using $\mathbf{A}_a$, and translating it using $\mathbf{T}_m$, so that a shearlet system can be defined as:

$$S(\varphi) = \mathbf{A}_a \cdot \mathbf{S}_s \cdot \mathbf{T}_m \cdot \varphi \quad . \tag{1}$$

Shearlet systems can be regarded as consisting of certain generating functions whose resolution is changed by a parabolic scaling matrix $\mathbf{A}_{2j}$ or $\tilde{\mathbf{A}}_{2j}$ defined by:

$$\mathbf{A}_{2j} = \begin{pmatrix} a^j & 0 \\ 0 & a^{j/2} \end{pmatrix} \quad \text{and} \quad \tilde{\mathbf{A}}_{2j} = \begin{pmatrix} a^{j/2} & 0 \\ 0 & a^j \end{pmatrix} \quad . \tag{2}$$

Equal scaling along both axes will not be able to capture anisotropic features, hence different scaling for the axes is required.

Although other ratios for scaling the axes are possible, this choice, known as parabolic scaling, optimizes the approximation properties for the piecewise smooth image model considered. To change the orientation of the generating function, an obvious choice is a rotation operator. However, rotations destroy the integer lattice (except for trivial rotations that switch the axes). In other words, integer locations may get mapped to fractional locations after a rotation. This leads to the problem of obtaining a discrete transform that is consistent with the continuous transform (where approximation properties have been optimized). As an alternative orientation operator, the orientation is changed by a shearling matrix:

$$\mathbf{S}_k = \begin{pmatrix} 1 & s \\ & \\ 1 & s \end{pmatrix} . \tag{3}$$

This achieves orientation changes using the slope s rather than a rotation angle. It has the advantage of leaving the integer lattice invariant when s is chosen as an integer.

Finally, a translation operator is defined that shifts the generating function:

$$\mathbf{T}_m(\varphi) \rightarrow \varphi(t - m) . \tag{4}$$

The conditions on the generating function so that the shearlet system $S(\varphi)$ can represent any square-integrable function, are known as admissibility conditions.

To investigate the differences of wavelet, curvelet and shearlet, we show the frequency tiling of three multiscale transform in Fig. 1. Here we can see:

1. Meyer wavelet: Regularization wavelets may well represent isotropic data.

2. Curvelet: Tight directional support frame, fine-scale data can be a good representation of anisotropy. However, curvelets offer limited localization in the spatial domain since they are band limited.

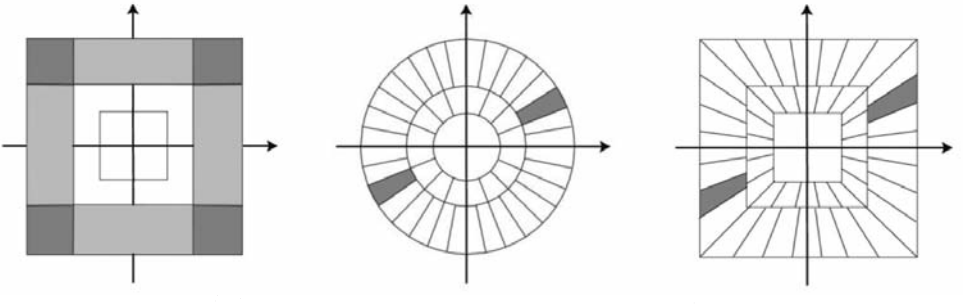

(a) (b) (c)

Fig. 1. The frequency tiling of a) wavelet, b) curvelet, c) shearlet.

3. Shearlet: Compactly directional support frame, fine-scale data can be a good representation of anisotropy, provides a unified treatment of continuous as well as discrete models, allowing optimally sparse representations of piecewise smooth images.

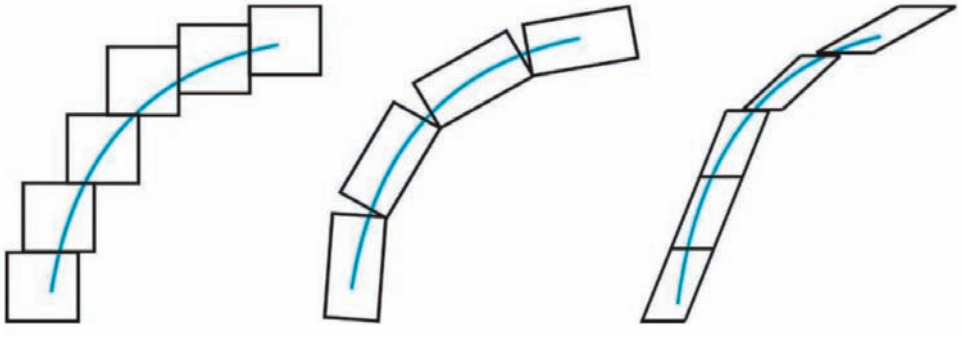

(a) (b) (c)

Fig. 2. Anisotropically scaled and sheared atoms efficiently cover curve-like singularities, a) wavelet, b) curvelet, c) shearlet.

SEISMIC DECONVOLUTION WITH SHEARLET SPARSITY CONSTRAINED INVERSION

The forward problem of seismic data deconvolution can be written as:

$$s = w * r + n \ , \tag{5}$$

where s represents the data, r represents the reflectivity, w represents the source wavelet and n represents zeros-centered white Gaussian noise, respectively. The symbol $*$ denotes linear convolution. The only quantity we know is the seismic data, and the source wavelet can be estimated by other ways. These are two knowns to search the other one unknown if we ignore the noise data. We rewrite eq. (5) as:

$$s = \mathbf{W}x + n \ , \tag{6}$$

where $\mathbf{W}$ denotes a $N \times M$ wavelet matrix, whose elements are $\mathbf{W}_{ij} = w_{i-r+1}$, and the deconvolution problem become given s and $\mathbf{W}$ to find the reflectivity x.

A simple way is to find $\mathbf{W}^{-1}$, so that the approximate solution of x can be written as:

$$\tilde{x} = \mathbf{W}^{-1}s = x + \mathbf{W}^{-1}n \ . \tag{7}$$

Deconvolution is an ill-posed problem, and moreover, the large changing range of $\mathbf{W}^{-1}$ makes a large deviation between the calculated $\tilde{\mathbf{r}}$ and real $\mathbf{r}$.

Since the 1980's, many researchers express this problem as an l_1-norm minimization:

$$\tilde{x} = \arg\min_x \|x\|_1 \quad \text{s.t.} \quad \|\mathbf{W}x - y\|_2 \leq \varepsilon \ , \tag{8}$$

where $\tilde{x}$ represents the estimated reflectivity vector, $\mathbf{W}$ is the deconvolution operator of the source wavelet, y is the data and ε is the noise level.

Eq. (8) means estimating a set of reflectivity coefficients with a minimum l_1-norm, and the set of coefficients satisfies the condition that the l_2-norm of the misfit between seismic data and the $\mathbf{W}x$ less than a certain noise level. By controlling the sparsity of reflectivity with the l_1-norm and the noise error with the l_2-norm, the approximation reflectivity can be obtained. This algorithm has relatively improved the accuracy of the deconvolution, but it is required that the reflectivity is sparse, and its solving process is a single channel circular convolution, which may damage the continuity of formation. To some extent, this also enhances the noise and reduces the signal-to-noise ratio.

In this paper, we do not need to assume that the reflectivity coefficients is sparse. By transforming the coefficients into Shearlet domain, the sparse reflectivity is represented by sparse shearlet coefficients. We introduce the shearlet operator into eq. (4) and rewrite it as:

$$\begin{cases} \tilde{x} = \arg\min_x \|x\|_1 \quad \text{s.t.} \quad \|\mathbf{W}x - y\|_2 \leq \varepsilon \\ \tilde{r} = S^T \tilde{x} \end{cases} , \tag{9}$$

where $\tilde{x}$ denotes the shearlet coefficients of the reflectivity vector, $\mathbf{W}$ represents the deconvolution operator of the source wavelet, S^T is the inverse shearlet operator, y is the data. The estimated reflectivity coefficient is $\tilde{r} = S^T \tilde{x}$.

Through eq. (9) we combine the Shearlet transform with deconvolution, which calculating a set of minimum sparse Shearlet coefficients with the l_1-norm. In this process, total reflectivity coefficients is used to approximate the true reflectivity coefficients in the Shearlet domain. In this way we can keep the formation reflector inherent continuity. According to the sparsity of the Shearlet transform, the main seismic reflector concentrates to a few large shearlet coefficients, while white noise remains by itself with low amplitude after a transform on any orthogonal basis. So the shearlet coefficients of the signal is relatively greater than that of noise. We can remove the noise by applying threshold, and improve the anti-noise ability of the algorithm.

In order to solve eq. (9), we describe the solving sparse reflectivity coefficients problem as the objective function consisting error with the l_2-norm and the solution with the l_1-norm:

$$J = \tfrac{1}{2}\| WR - y \|_2^2 + \lambda \| r \|_1^1 = \tfrac{1}{2}\| WS^T x - y \|_2^2 + \lambda \| x \|_1^1 \quad , \qquad (10)$$

where $\| g \|_2^2$ and $\| g \|_1^1$ represent the l_2-norm and the l_1-norm separately, λ is the trade-off parameter to balance the weight or impact of the two terms; the larger λ, the larger is the weight of the l_1-norm. The l_2-norm constrained is adopted to the first half of the cost function [eq. (10)].

In this paper, we chose fast iterative shrinkage thresholding algorithm (FISTA) to solve eq. (10). Pérez et al. (2013) combined FISTA and a standard least-squares algorithm to solve the amplitude-versus-angle inversion problem. FISTA can be viewed as an extension of iterative shrinkage thresholding algorithm (ISTA). ISTA is a kind of attractive linear inversion technique due to its simplicity and thus is adequate for solving large scale problems. However its low convergent rate seriously limits the computational efficiency. ISTA defines an iteration formula of soft threshold to calculate x in eq. (10):

$$x_k = T[x_k - 2t(y - Ax_k)] \quad . \qquad (11)$$

In our deconvolution problem we rewrite it as:

$$x_k = T[x_k + (1/\alpha)(WS^T)^T(y - WSx_k),(\lambda/\alpha)] \quad , \qquad (12)$$

where y is an intermediate variable, λ and α are two parameters. W is the deconvolution operator of the source wavelet, S is the forward Shearlet transform operator, S^T is the inverse Shearlet transform operator.

The threshold is controlled by adjusting α. The soft thresholding function we use is:

$$T(x) = \begin{cases} x - \text{sign}(x) & \text{if } |x| \geq \lambda \\ 0 & \text{if } |x| < \lambda \end{cases} \quad . \qquad (13)$$

By changing x, FISTA improved the convergence speed significantly. The new x_k is not calculated by the previous point x_{k-1}, but uses a very specific linear combination of the previous two points $\{x_{k-1}, x_{k-2}\}$:

$$x_{k+1} = x_k + (t_{k-1}/t_{k+1})(x_k - x_{k-1}) \quad , \qquad (14)$$

$$t_{k+1} = [1 + \sqrt{(1+4t_k^2)}]/2 \quad . \qquad (15)$$

FISTA preserves the computational simplicity of ISTA but with a global rate of convergence. It is very suitable for solving problems of the very large scale data such as seismic data.

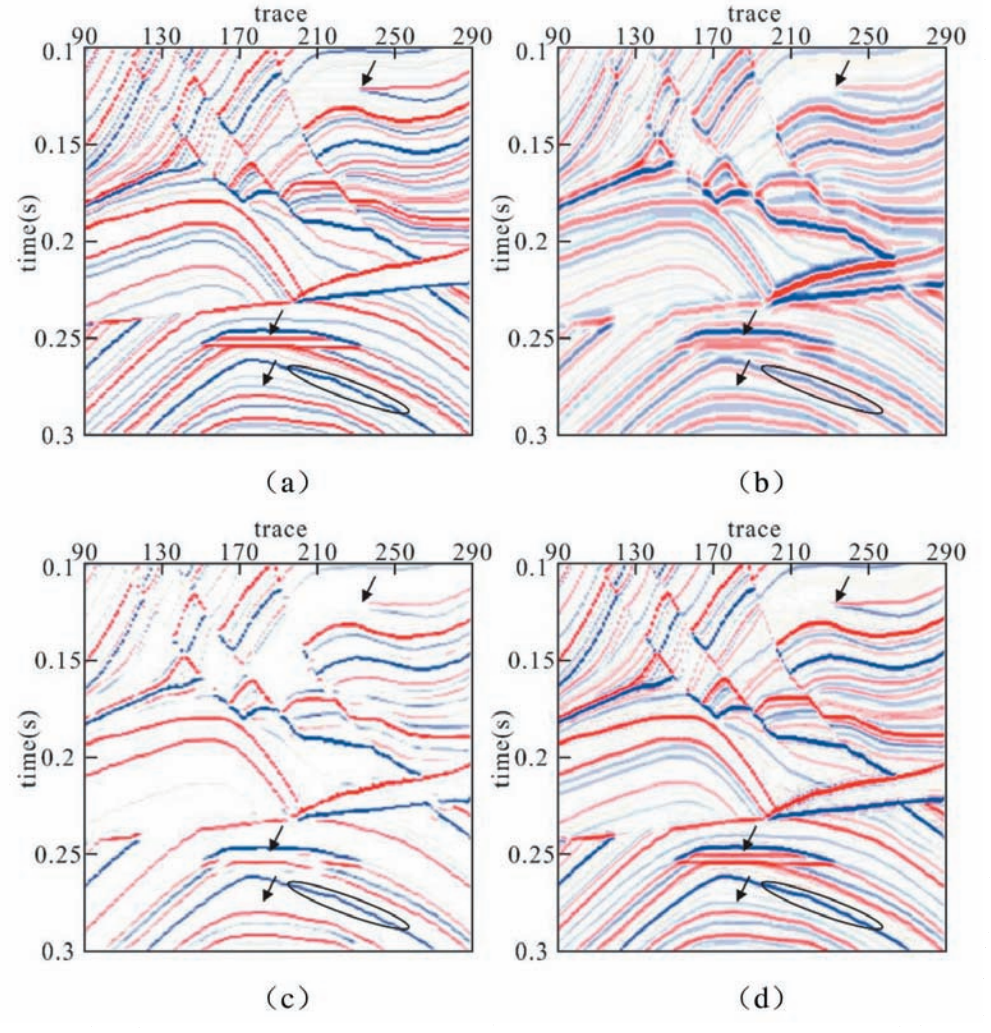

Fig. 3. Experiment on a complex model. a) The reflectivity model. b) Synthetic seismic data. c) Estimated reflectivity with sparse spike deconvolution. d) Estimated reflectivity with Shearlet deconvolution.

EXAMPLES WITH COMPLEX MODEL AND NOISE DATA

To investigate the ability of deconvolution based on shearlet sparsity constrained inversion, we carry out an experiment on a complex geological model. The reflectivity model is part of the Marmousi model. Seismic data is obtained by convolving a Ricker wavelet (central frequency = 25 Hz) with the reflectivity. We applied sparse spike deconvolution and shearlet deconvolution to estimate reflectivities. Figs. 3a and 3b show the reflectivity model and the corresponding synthetic seismic data. Four labels in Fig. 3 highlight the better performance of the proposed method. The first arrow located around 0.12 s indicates a wedge geological model. The second arrow located around 0.25 s indicates a thin interbed reservoir model. The third arrow located around 0.27s indicates a weak reflectivity model. The ellipse shows a rough reflectivity. Due to the tuning effect of the wavelet, the wedge model becomes blurred and indistinct, the thin interbed reservoir is almost invisible in Fig. 3b.

Figs. 3c and 3d show the results of sparse spike deconvolution and our algorithm respectively for the synthetic data. In Figs. 3c and 3d, both algorithms improve resolution. However, in Fig. 3c the sparse spike deconvolution does not clearly express the wedge geological model, the two coherent events separate from each other. Moreover, the thin interbed reservoirs as well as weak reflectivity turn out to have disappeared. In Fig. 3d, shearlet deconvolution estimates an accurate result. The wedge geological model resembles the true model, and we can clearly recognize the thin interbed reservoirs and weak reflectivity. Besides, shearlet deconvolution utilizes a multi-trace algorithm, exploits the structure in both time and spatial coordinate, which keep the continuity of events. Sparse spike deconvolution is a trace-by-trace operation, which does not account for the two-dimensional structure of the reflectivity model. In the ellipse marker, the reflectivity estimated by shearlet deconvolution is more smooth than that of sparse spiking deconvolution. Shearlet deconvolution estimated reflectors are structurally close to the true model.

In Fig. 4a, we add strong Gaussian white noise to the synthetic data. Fig. 4b and 4c show the estimated reflectivity by sparse spike deconvolution and shearlet deconvolution, respectively. The sensitive to noise and single trace processing make the sparse spike deconvolution result discontinuity. While the shearlet has an optimal sparse representation of the seismic data, the shearlet coefficients of noise energy is small. Combined with the FISTA algorithm, shearlet deconvolution can reduce the effect of random noise and improve the signal to noise ratio at the same time. The technique achieves excellent noise attenuation without removing any coherent events. As marked in Fig. 4c, the small geological structure still can be recognized.

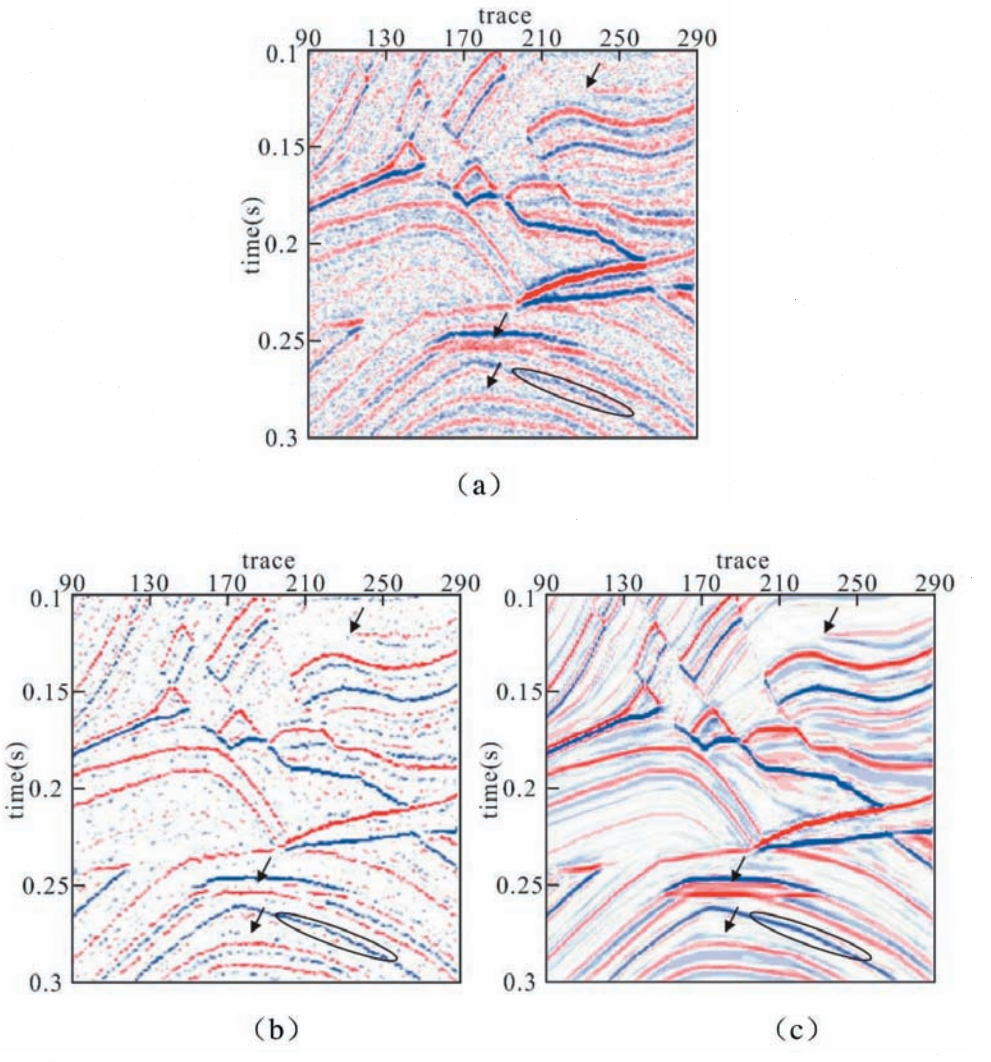

Fig. 4. Examples on noise data (SNR = 2.8828 dB). a) Noise data. b) Estimated reflectivity with sparse spike deconvolution. c) Estimated reflectivity with shearlet deconvolution.

FIELD DATA EXAMPLES

To verify the shearlet deconvolution on field data, we applied the proposed method on a post-stack seismic data. The data has 400 traces, and every trace has 400 samples. The wavelet used is estimated with high order statistic method.

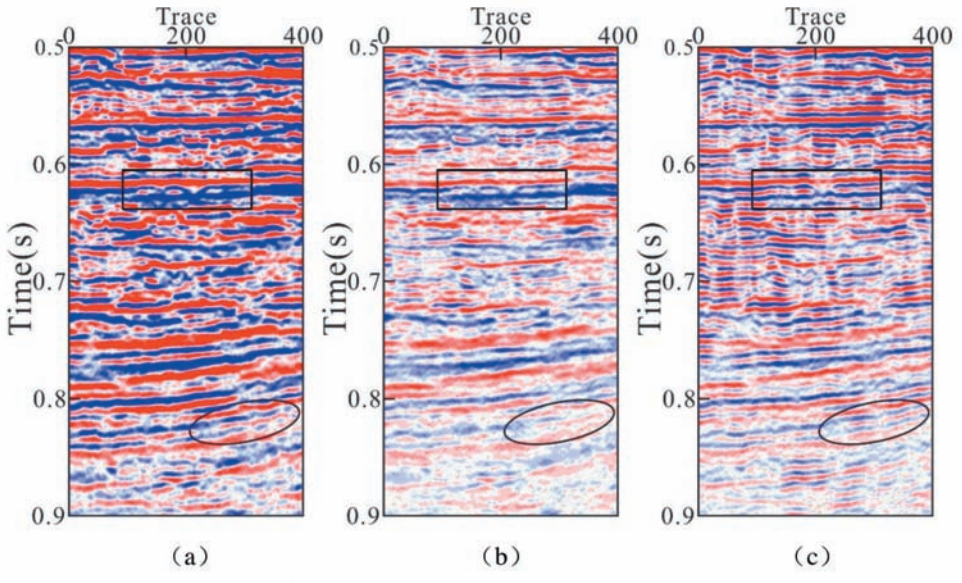

Fig. 5. Examples on field data. a) Original seismic data. b) Estimated reflectivity with sparse deconvolution. c) Estimated reflectivity with Shearlet deconvolution.

Fig. 5a is the original seismic data. Because of the stratum absorption, high-frequency signals are absorbed. The rectangular located around 0.63 s indicate a thin layer, it is difficult to distinguish from the original profile. Both sparse spike deconvolution and shearlet deconvolution are applied. We get some improves by sparse spike deconvolution, but still cannot recognize the thin layers. As we can see in Fig. 5c, two events could be clearly recognized by the Shearlet sparsity constrained deconvolution. Seismic profile is always discontinuity in deeper area because of weak energy. Comparing the highlighted ellipse in Figs. 5c and 5b, it is obvious to find that the proposed technique is capable to improve the resolution and keep the seismic events continuity as well.

Fig. 6a shows the frequency spectrum of original data. The spectrum decays rapidly after 60 Hz. Fig. 6b shows an improved spectrum after 60 Hz with sparse spike deconvolution, Fig. 6c shows spectrum with shearlet deconvolution. In Fig. 6c the spectrum is improved not only after 60 Hz, but also at low frequency. Results show our method can expand the spectrum band efficiently.

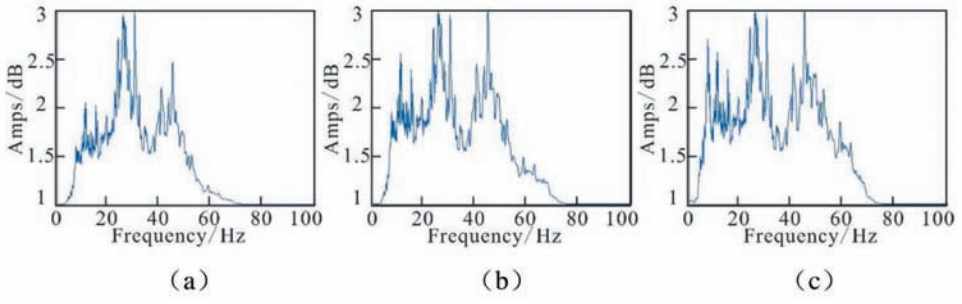

Fig. 6. The corresponding spectrum of Fig. 5. a) Field data. b) Sparse deconvolution. c) Shearlet deconvolution.

CONCLUSIONS

In this paper, we proposed a seismic deconvolution algorithm based on shearlet sparse constrained inversion. The sparse reflectivity is represented by the sparse shearlet coefficients, making the deconvolution results more smoothly. Deconvolution based on multi-dimensional space transform instead of the traditional single channel deconvolution, can keep the continuity of seismic signal in theoretically. We combine the deconvolution problem with norm and solving this problem by FISTA. In this way, our algorithm can attenuate noise and accelerate computational efficient. Synthetic and field data examples show our algorithm is robust.

ACKNOWLEDGEMENTS

We thank the ShearLab for sharing their codes available on the web. This research is supported by the Major Projects of the National Science and Technology of China (Grant No. 2011ZX05023-005-008).

REFERENCES

Beck, A. and Teboulle, M., 2009. A fast iterative shrinkage-thresholding algorithm for linear inverse problems. SIAM J. Imaging Sci., 2: 183-202.

Berkhout, A.J., 1977. Least-squares inverse filtering and wavelet deconvolution. Geophysics, 42: 1369-1383.

Canadas, G., 2002. A mathematical framework for blind deconvolution inversion problems. Expanded Abstr., 72nd Ann. Internat. SEG Mtg., Salt Lake City: 2202 -2205.

Claerbout, J.F. and Muir, F., 1973. Robust modeling with erratic data. Geophysics, 38: 826-844.

Gray, W., 1979. Variable Norm Deconvolution. Ph.D. thesis, Stanford University, Stanford. !!!!!

Guo, K. and Labate, D., 2007. Optimally sparse multidimensional representations using shearlets. SIAM J. Mathemat. Anal., 39: 298-318.

Hennenfent, G., Herrmann, F.J. and Neelamani, R., 2005. Seismic deconvolution revisited with curvelet frames. Extended Abstr., 67th EAGE Conf., Madrid.

Herrmann, F.J., 2005. Seismic deconvolution by atomic decomposition: A parametric approach with sparseness constraints. Integr. Computer-Aided Engin., 12: 69-90.

Kaaresen, K.F. and Taxt, T., 1998. Multichannel blind deconvolution of seismic signals. Geophysics, 63: 2093-2107.

Labate, D. and Kutyniok, G., 2005. Sparse multidimensional representation using shearlets. Proc. SPIE - Internat. Soc. Optic. Engin., 5914: 254-262.

Meng, D.J. and Wang, D.L., 2013. Sparse deconvolution on the curvelet transform. Acta Petrol. Sin., 34: 107-114.

Nojadeh, N.K. and Sacchi, M.D., 2013. Wavelet estimation via sparse multichannel blind deconvolution. Extended Abstr., 75th EAGE Conf., London.

Oldenburg, D.W., Levy, S. and Whittall, K.P., 2012. Wavelet estimation and deconvolution. Geophysics, 46(11): 1528-1542.

Pérez, D.O., Velis, D.R. and Sacchi, M.D., 2013. High-resolution prestack seismic inversion using a hybrid FISTA least-squares strategy. Geophysics, 78(5): R185-R195.

Shlomo, L. and Peter, K.F., 1981. Reconstruction of a sparse spike train from a portion of its spectrum and application to high-resolution deconvolution. Geophysics, 46: 1235-1243.

Ulrych, T.J., 1971. Application of homomorphic deconvolution to seismology. Geophysics, 36: 650-660.